Viser Technology Pte. Ltd.
Research and Application of Materials Science
DOI: 10.33142/rams.v4i1.8462

Research Article Open Access

One dimensional terpyridine-based metal organic framework for stable supercapacitor

Haoxuan FENG, Weiqi LI, Chenyu MA *, Haiyan HE

College of Mechanics and Materials, Hohai University, Nanjing, Jiangsu, 210098, China

***Corresponding Author:** Chenyu MA, E-mail addresses: chenyuma1999@163.com*

Abstract:
In summary, a novel structure of MOF based on 1,4–di ([2,2':6',2"terpyridin] -4'-yl)benzene and 1,4-naphthalenedicarboxylic acid has been constructed through hydrothermal reaction. The Ni-MOF displays one dimensional zigzag chain, which connect each other by hydrogen bonding to form three dimensional supramolecule with large channels. The conjugated systems of the terpyridin and benzene ligands enhance the chain rigidity, accelerate the electron transport. The massive channels provides electrolyte rapid transfer. By the structural feature aforementioned, the Ni-MOF demonstrates stable electrochemical performance as suprocapacitor.
Keywords: *suprocapacitor; metal-organic framework; supramolecule; terpyridin; hydrothermal reaction*

1 Introduction

In recent years, with the decline of non-renewable resources and the global demands for clean energy shortage, the development of clean and efficient energy storage equipment has become an important research direction. However, chemical and physical limitations of existing materials hinder performance and require new solutions. For instance, polymers and conductive carbon materials are relatively inexpensive, scalable, and synthetically tunable but can lack physical and chemical stability for device implementation. On the other hand, solid inorganic materials, such as metal oxides and silicon, are used as electrode materials due to their robust structure and redox-active sites. However, sluggish ion diffusion of metal oxides limit charge discharge rate capabilities and large volumetric changes lead to mechanical instability [1]. Metal Organic Frameworks are one reasonable type of materials to solve the above issues due to their metal atoms and organic skeletons, adjustable channels and extraordinary porosity, which display different applications by diverse metal atoms [2-4]. MOFs are entering the limelight as supercapacitors by virture of the tunable structure, large specific surface area and amount of accessible active centers [5-7]. Meanwhile, MOFs materials can be used as redox centers of pseudo-capacitors, which can accelerate the reaction because of their skeleton structure and many active sites.

Supercapacitors have two main mechanism: a double-layer capacitor and a pseudo-capacitor [8-10]. Double-layer capacitor works on the principle that during charging, ions with opposite charges accumulate on the electrode surface and are stored between the electrodes and electrolytes. The double-layer capacitor has good invertibility and power density because of its fast electrochemical reaction near the surface. The pseudo-capacitorsused in this paper is mainly charged and discharged through the rapid oxidation-reduction reaction on the electrode surface, which reflects well the efficiency of the supercapacitor because of the rapid reaction [11-13]. Due to the high specific surface area of carbon materials, activated carbon, carbon nanotubes and graphene are commonly used as electrode materials in current research. Despite carbon materials have such excellent characteristics, they are not necessarily suitable for supercapacitors. For example, Chao Feng et al. reported a Ni-MOF material with a specific capacitance of 184 F/g at a rate of 5 mV/s [14]. Yue et al reported a kind of Zn-MOF used in supercapacitors. At the current density of 0.5 A/g, the specific capacitance is only 138 F/g[15]. When these materials are used as supercapacitors, they have no good energy storage effect because of their small specific capacitance. Chao Feng et al. reported a Ni-MOF material has lost a lot of specific capacitance under 1000 cycles [16-17].A kind of MOFs used in supercapacitor is reported by Kong et al. After 1000 charge-discharge cycles, the specific capacitance keeps only 72.8% [18]. It indicates that the MOFs material has short service life when used as a supercapacitor, which does not accord with the characteristics of long service life of supercapacitors. While some MOFs have high

Received on March 11, 2022; Accepted on April 18, 2022

specific capacitance and good cycle stability when they are used as supercapacitors, they will lose large specific capacitance when they are used as supercapacitors at high current density. When the material is used as a supercapacitor, the specific capacitance can only keep 71.21% at the current density of 10 A/g at Kang Liu et al.'s paper [19]. At the current density of 20 A/g, the specific capacitance of Zhu et al supercapacitor is only 47.2% [20].

Based on the above question, a Ni-based MOFs material was synthesized by in-situ reaction and its structure was characterized in this paper. The electrochemical performance of the supercapacitor was also evaluated.

2 Experimental section

2.1 Synthesis of HU17

All the reagents were purchased and used directly without further purification, Ni-MOF was synthesized by hydrothermal method, 0.02 g of $Ni(NO_3)_2$, 0.001g of 1,4-di([2,2':6',2"terpyridin]-4'-yl)benzene (1,4-Tpb), 0.005g of 1,4-naphthalenedicarboxylic acid (1,4-Npa) with a balance, and then mixing them with 5 ml distilled water. The glass bottle is put into the plastic inner liner, and then the inner liner is put into the sealed reactor. It was cooled naturally after 72 hours reaction at 150 ℃. If all the impurities are yellow dendritic crystals and a few yellow massive crystals, they will be regarded as pure. The product was extracted into the sample tube and dried in a 50 ℃ constant temperature oven to obtain the required crystals.

2.2 Single-crystal structure determination

The single crystal HU17 was diffracted by Agilent SuperNova X-ray diffractometer at 298K(radiation type is MOK/a, radiation wavelength is 0.71 Å). The crystal table is shown in Table 1.

2.3 Electrochemical measurements

Two rectangular nickel foams with the same shape and similar size are cut and it's twice as long as it's wide. First weighing the quality of two pieces of nickel foam, removing one nickel foam and setting the balance to zero, the sample is 2.5 mg at the end of the remaining nickel foam. Cover with another nickel foam, wrap it in weighing paper, and put it into a tablet press.

In this paper, three-electrode test is used. Pt sheet is used as the opposite electrode, the reference electrode is the saturated calomel electrode, and the working electrode is the MOFs material electrode. The electrolyte solution is 6 Mol/L KOH.

2.3.1Cyclic voltammeters:

The specific capacitance of electrode material is measured by cyclic voltammetry. The formula is

$$C = \frac{\int \mathrm{idu}}{\mathrm{mv}\triangle V} \quad (1)$$

Among them, C is the specific capacitance (F/g), m is the mass (g) of MOFs, △V is the Window voltage (V), i is the current intensity (A), and v is the scanning rate (mV/s)[21].

We can get different specific capacitance by changing the scanning rate v.

2.3.2Constant current charge and discharge test:

Constant current charging and discharging is to use constant current to test electrode material. The formulais

$$C = \frac{I\triangle \mathrm{t}}{\mathrm{m}\triangle V} \quad (2)$$

Among them, C is the specific capacitance (F/g), m is the mass (g) of MOFs, △t is the Discharge time (s), I is the current intensity (A), and △V is Window voltage (V)[22-23].

We can obtain specific capacitance at different current by changing current.

2.3.3Impedance test:

Two test voltages are set, one is 0.45 V, and the other is the voltage corresponding to the oxidation peak in the CV curve. Test frequency is 0.01 Hz-100KHz.

Table 1 Crystal date and structure refinement for complexes HU17

complex	HU17
empirical formula	C60 H42 N6 O11 Ni2
formula weight	1140.41
T (K)	293.15
crystal system	triclinic
space group	P1 2/n1 (13)
a (Å)	11.4409 (8)
b (Å)	14.8757 (9)
c (Å)	17.6457 (11)
α (°)	74.092 (2)
β (°)	76.830 (2)
γ (°)	79.855 (2)
V (Å 3)	2791.4 (3)
Z	2
Dc (Mg ·mm-3)	1.357
μ (mm-1)	0.740
F (000)	1176
index ranges (h, k, l)	-13/13 -17/17 -21/20
reflections collected	7049
Rint	0.0481
restraints/parameters	0/716
GOF (F2)	1.009
R1,wR2 [I > 2σ(I)]a	0.0547, 0.1333
R1,wR2 (all data)b	0.0896, 0.1445
Largest diff. peak/hole (e ·Å-3)	0.413, - 0.304

a R1 = Σ| |Fo|-|Fc| |/ Σ|Fo|

b wR2 = [Σw(Fo2-Fc2)2]/ Σw(Fo2)2]1/2

3 Results and discussion

3.1 Crystal structure of HU17

A novel structure of MOF based on 1,4-di([2,2':6',2"terpyridin] -4'-yl)benzene (1,4-Tpb) and 1,4-naphthalenedicarboxylic acid (1,4-Npa) has been constructed by solvothermal reaction. The asymmetric unit contains two central atoms (Ni1 and Ni2), one1,4-Npa ligand, one 1,4-Tpb ligand, and three coordinated water molecules. As can be seen from the Figure 1, the central atom Ni has two coordination environments. Figure 1(a) shows the Ni1 is a tridentate chelate with a 1,4-Tpb, one 1,4-Npa and two H2O. Figure 1(b) shows the Ni2 is a tridentate chelate with a 1,4-Tpb, one H2O and two 1,4-Npa, respectively. The asymmetric units are directly connected to form a chain. 1,4-Npa presents two coordination environments, one is bridged with two metal center ions Ni, as shown in Figure 1(c); the other is bridged with only one metal center ion Ni, as shown in Figure 1(d). There is only one coordination environment for 1,4-Tpb, that is, the two ends are tridentate chelate with two metal center ions Ni. Figure 1(f) shows the asymmetric unit of complex HU17. It is composed of two units in Figure 1 connected by a common 1,4-Npa. Figure 1 (g) shows the molecular chain of HU17. It is composed of asymmetric units connected. Figure 1(h) is a schematic diagram of the connections between different chains. From the figure, we can see that there is no link between the chain and the chain. Considering the hydrogen bonds with an average distance of 2.67 Å, two parallel chains connected to form a supramolecule network. Figure 1(i) is a schematic diagram of the connection modes of adjacent network structures. The adjacent mesh structures are connected to each other form three-dimensional structures. There are some independent water molecules occupied the channels of these chains.

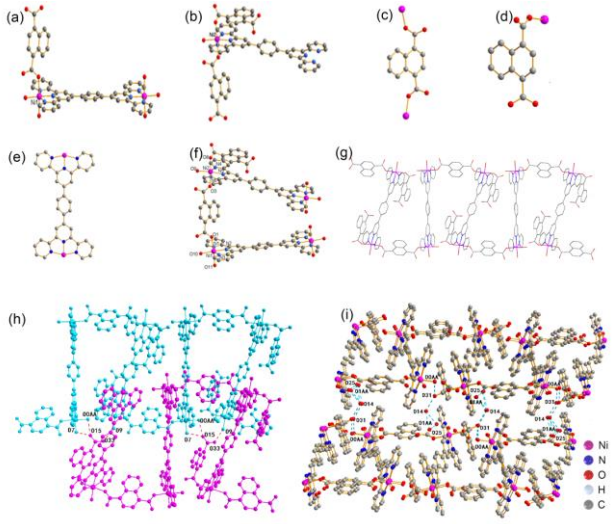

Figure 1 (a) Coordination environment of Ni1; (b) coordination environment of Ni2; (c) and (d) the coordination modes of 1,4-Npa; (e) the bridging mode of 1,4-Tpb; (f) an asymmetric unit of HU17, (g) the single chain structure of HU17; (h) The hydrogen bonds between two chains; (i) The 3D network of HU17

Figure 2 shows the thermogravimetric curve of HU17. It can be seen from the figure that in the range of 0 to 300 ℃, the complex HU17 loses 7% of its mass, which is a process of gradually losing crystal water .In the range of 300 to 780℃, the mass of the complex HU17 is greatly reduced, and 80% of the total mass is lost, because its crystal skeleton is gradually oxidized and decomposed. Above 780℃, the mass increases slightly because the metal is oxidized to metal oxides.

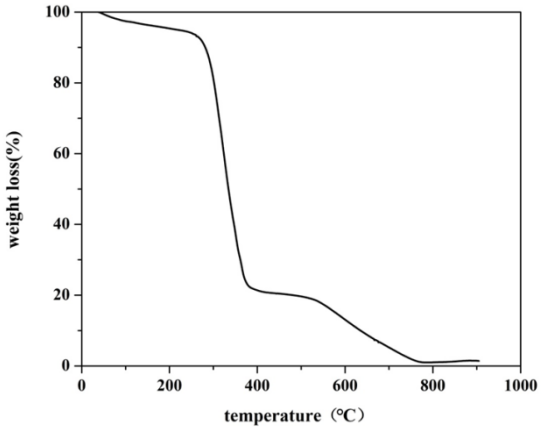

Figure 2 Thermogravimetry analysis of HU17

The GCD curve is shown in Figure 3(a). The current density gradually increased from 1 A/g to 20 A/g. with the increase of current density, the charging and discharging time became shorter and the curve compressed to the ordinate. According to formula b, the specific capacitance of complex HU17 can be calculated. The calculated results are represented by histogram, and the schematic diagram of specific capacitance is Figure 3(c). As can be seen from Figure 3(c), with the increase of current density, the specific capacitance decreases gradually. This is because under the large current density, the charging and discharging time decreases, and all active sites cannot be fully called, so that some active sites are not involved in the charging and discharging, resulting in the reduction of specific capacitance. At the current densities of 1 A/g, 2 A/g, 5 A/g, 10 A/g, 15 A/g and 20 A/g, the specific capacitances are 135.5, 132.4, 127.5, 122.4, 121.6 and 117.2 F/g, respectively. It can be seen that the specific capacitances at 20 A/g and 1 A/g current densities are only 13.5% compared with each other, indicating that the complex HU17 has a faster reaction rate when it is used as a super capacitor, which conforms to the characteristics of fast charging of super capacitor.

Figure 3(b) is the CV test curve. It can be seen from the figure that in the cyclic voltammetry test, the super capacitor has oxidation peak and reduction peak, indicating that the super capacitor is a Faraday capacitor. At the same time, we can see that with the increase of scanning rate, the curve deforms to a certain extent,

which shows that the capacitor becomes unstable under high scanning rate. Formula a can be used to calculate the specific capacitance of materials at different scanning rates, and the specific capacitance is displayed by histogram. At the scanning rates of 1 mV/s, 2 mV/s, 4 MV/s, 6 MV/s, 8 MV/s, and 10 mV/s, the specific capacitance is 332.8, 314.7, 294.8, 283, 274.8, 268.9 and 258.6 F/g, respectively. It can be seen that at the scanning rate of 1 mV/s, the material has high specific capacitance, which is in line with the characteristics of high capacitance of super capacitor. At the same time, it can also be seen that the specific capacitance loss rate is only 22.3% at the scanning rate of 20 mV/s and 1 mV/s, that is to say, at the high scanning rate, the electrode material can still maintain a high efficiency, which shows that the electrode material has good stability at high scanning speed.

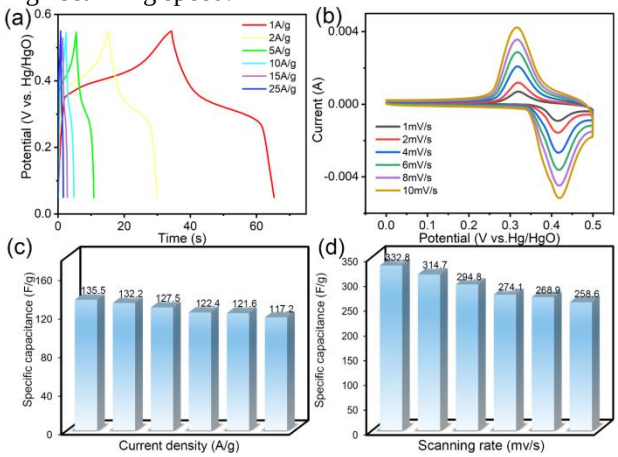

Figure 3 (a) The GCD curve of HU17, (b) the CV curve of HU17, (c) the specific capacitance measured under GCD curves, and (d) the specific capacitance measured under CV curves

The EIS curve of this MOF electrode material is shown in Figure 4 Curve 1 is 0.45V, and Curve 2 is the voltage corresponding to the oxidation peak in the CV curve. From Figure 4(b), it can be seen that the HU17 electrode material has a small semicircle in the high frequency region, which indicates that the electrode material has a small internal resistance. In Figure 4(a), it can be seen that the slope of HU17 electrode material is small in the low frequency region, which indicates that the electron transfer rate of HU17 electrode material is not very fast.

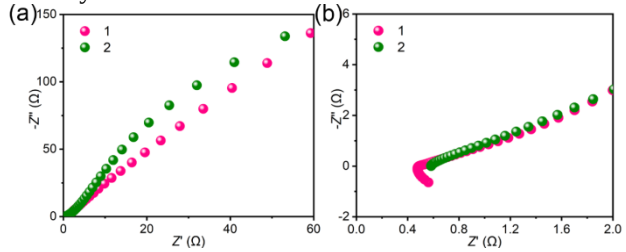

Figure 4 (a) The low frequency zone of EIS Curve and (b) the high frequency zone of EIS curve

Figure 5 shows the cyclic stability curve of HU17 for supercapacitors. It can be seen that the capacitance efficiency of the electrode material can remain 100% after 10000 charge-discharge cycles. This indicates that HU17 has excellent cyclic life for supercapacitors and is suitable for supercapacitors.

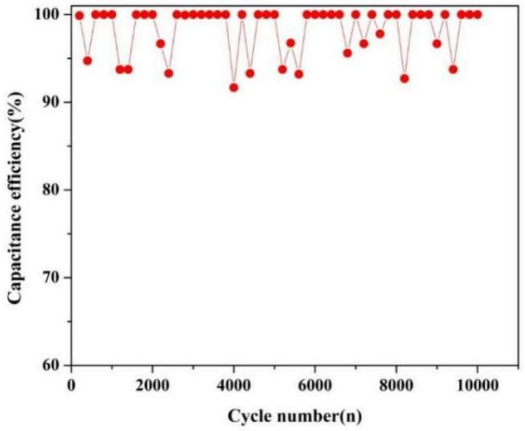

Figure 5 The cyclic stability curve of HU17

4 Conclusions

In summary, a novel structure of MOF based on 1,4–di ([2,2':6',2"terpyridin] -4'-yl)benzene and 1,4-naphthalenedicarboxylic acid has been constructed. The Ni-MOF displays one dimensional zigzag chain, which connect each other by hydrogen bonding to form three dimensional supramolecule with large channels. The conjugated system of the terpyridin and benzene ligands enhance the chain rigidity, accelerate the electron transport. The massive channels provides electrolyte rapid transfer. By the structural feature aforementioned, the Ni-MOF demonstrates stable electrochemical performance as suprocapacitor.

Acknowledgments

This work was financially supported by the National Natural Science Foundation of China (22209037) and the Fundamental Research Funds for the Central Universities (No. B220202042).

References

[1] E. Baumann, A. Burns, Q. Liu, et al. Metal-organic framework functionalization and design strategies for advanced electrochemical energy storage devices, Commun. Chem. 2019(2): 13.

[2] H. Furukawa, E. Cordova, M. O'Keeffe, et al. The chemistry and applications of metal-organic frameworks, Science. 2013(341): 1230444.

[3] X. Du, W. Cai, Q. Zhang, et al. Rhodium nanoflowers on three-dimensional graphitic carbon nitride nanosheets/graphene hybrid aerogels as electrocatalysts for methanol oxidation, ACS Appl. Nano Mater. 2021(4): 9729–9737.

[4] J. Qin, H. Huang, J. Zhang, et al. Stereoassembly of

ultrasmall Rh-decorated zeolite imidazolate framework–MXene heterostructures for boosted methanol oxidation reaction, J. Mater. Chem. A 2023(11): 2848-2856.

[5] D. Sheberla, J. Bachman, J. Elias, et al. Conductive MOF electrodes for stable supercapacitors with high areal capacitance, Nat. Mater. 2017(16):220-224.

[6] L. Wang, X. Feng, L. Ren, et al. Flexible solid-state supercapacitor based on a metal-organic framework interwoven by electrochemically-deposited PANI, J. Am. Chem. Soc. 2015(137):4920-4923.

[7] R. Salunkhe, Y. Kaneti, J. Kim, J. Kim, Y. Yamauchi, Nanoarchitectures for metal-organic framework-derived nanoporous carbons toward supercapacitor applications, Acc.Chem. Res. 49 (2016):2796-2806.

[8] G. Wang, L. Zhang, J. Zhang. A review of electrode materials for electrochemical supercapacitors, Chem. Soc. Rev. 2012(41):797-828.

[9] P. Simon, Y. Gogotsi. Materials for electrochemical capacitors, Nat. Mater. 7 (2008) 845-854.

[10] R. Kotz, M. Carlen. Principles and applications of electrochemical capacitors, Electrochim. Acta. 2000(45):2483-2498.

[11] J. Qiu, Z. Bai, G. Dai, et al. NiO/Co_3O_4 nanoheterostructure derived from nickelocene filled ZIF-67 for supercapacitors, J Alloy. Compd. 2018(763): 966-974.

[12] J. Xu, Y. Wang, S. Cao, et al. Ultrathin Cu-MOF@δ-MnO_2 nanosheets for aqueous electrolyte-based high-voltage electrochemical capacitors, J. Mater. Chem. 2018(A 6): 17329-17336.

[13] Y. Zhang, R. Lin, Y. Fu, et al. Metal-organic framework derived Fe_2O_3 nanocubes on intertwined N-doped carbon nanowires for fiber-shaped supercapacitor, Mater. Lett. 2018(228): 9-12.

[14] X. Fang, B. Zong, S. Mao. Metal-organic framework-based sensors for environmental contaminant sensing, Nano-Micro Lett. 2018(10): 64.

[15] Y. Hou, L. Yan, X. Wang, et al. Excellent supercapacitor performance of robust nickel–organic framework materials achieved by tunable porosity, inner-cluster redox, and in situ fabrication with graphene oxide, Cryst. Growth Des. 2018(18): 6035-6045.

[16] C.Feng, P. Lv, Q. Li, et al. A porous 2D Ni-MOF material with a high supercapacitive performance, J. Solid State Chem. 2018(265): 244-247.

[17] H. Meng, B. Wan, P. Jiang, et al. Rodlike CeO_2/carbon nanocomposite derived from metal–organic frameworks for enhanced supercapacitor applications, J. Mater. Sci. 2018(53): 13966-13975.

[18] M. Yue, C. Yu, H. Duan, et al. Six isomorphous window-beam MOFs: explore the effects of metal ions on MOF-derived carbon for supercapacitors, Chem. 2018(24): 16160-16169.

[19] J. Kong, J. Zhu, W. Shuang, et al. Nitrogen-doped wrinkled carbon foils derived from MOF nanosheets for superior sodium storage, Adv. Energy Mater. 2018(8): 1-8.

[20] K. Liu, M. Deng, D. Li, et al. Two isostructural Co/Ni fluorine-containing metal-organic frameworks for dye adsorption and supercapacitor, J. Solid State Chem. 2019(275): 1-7.

[21] Z. Zhu, Z. Wang, Z. Yan, et al. Facile synthesis of MOF-derived porous spinel zinc manganese oxide/carbon nanorods hybrid materials for supercapacitor application, Ceram. Int. 2018(44): 20163-20169.

[22] R. Salunkhe, Y. Kamachi, N. Torad, et al. Fabrication of symmetric supercapacitors based on MOF-derived nanoporous carbons, J. Mater. Chem. 2014(A 2): 19848-19854.

[23] W. Xuan, R. Ramachandran, C. Zhao. F. Wang, Influence of synthesis temperature on cobalt metal-organic framework (Co-MOF) formation and its electrochemical performance towards supercapacitor electrodes, J. Solid State Electrochem. 2018(22): 3873-3881.